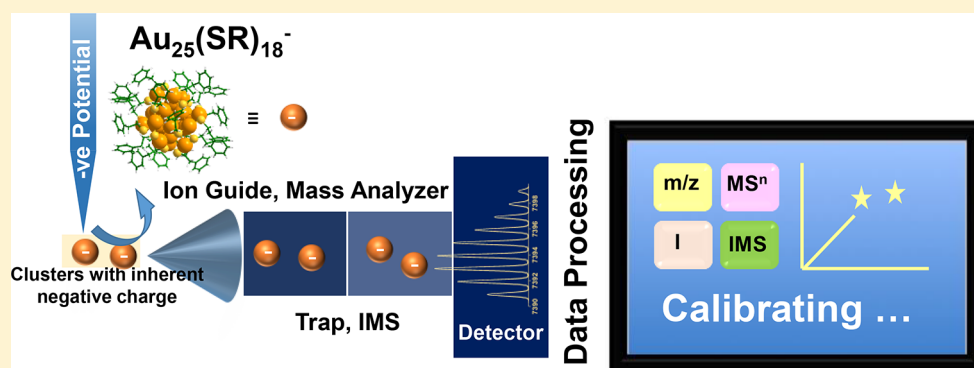


# Monolayer-Protected Noble-Metal Clusters as Potential Standards for Negative-Ion Mass Spectrometry

Ananya Baksi,<sup>†,‡</sup> Papri Chakraborty,<sup>‡</sup> Abhijit Nag, Debasmita Ghosh, Shridevi Bhat, and Thalappil Pradeep<sup>\*Ⓜ</sup>

DST Unit of Nanoscience and Thematic Unit of Excellence, Department of Chemistry, Indian Institute of Technology Madras, Chennai 600036, India

## Supporting Information



**ABSTRACT:** A detailed mass-spectrometric study of atomically precise monolayer-protected clusters revealed the potential application of such materials as mass-spectrometric standards, mostly in negative-ion mode and in the high-mass range. To date, very few molecules are known that can be efficiently ionized and detected at lower concentrations as negative ions with high signal intensities beyond  $m/z$  3000. Noble-metal clusters are molecules with definite masses, sizes, and shapes, which makes them excellent candidates to choose as standards over conventional low-molecular-weight polymers or clusters of ionic salts. They may be used as calibrants in all possible modes, including tandem mass spectrometry and ion mobility. With the advancement in materials science, more and more molecules are being added to the list that are inherently negatively charged in solution and can be examined by mass spectrometry. In this report, we demonstrate the use of three such model cluster systems for their potential to calibrate mass spectrometers in negative-ion mode. This idea can be extended to many other clusters known so far to achieve calibration in extended mass ranges.

Mass spectrometry (MS) has become an indispensable tool for the identification and characterization of organic molecules, proteins, and other biologically active species.<sup>1–4</sup> Pharmaceutical industries greatly depend on MS to determine the purity of drugs. In recent years, mass spectrometers have been used in hospitals and even during surgery.<sup>5–7</sup> It has proved to be a potential tool for biomarker identification for specific types of cancer.<sup>5</sup> The massive progress of MS in biology has prompted scientists to search for numerous proteins and peptides that can be used as standard molecules for understanding an unknown sample or calibrating instruments.<sup>4,8</sup> Most often, bigger proteins and peptides ionize reasonably well in positive-ion mode, and there are plenty of such molecules known to serve as mass-spectrometric standards.<sup>1,3,9</sup> Most of the protocols are commercialized and are being used throughout the world.

Although MS has deepened its roots in biology, it has also made a significant impact in materials science.<sup>2,10–13</sup> Recent developments in soft-ionization techniques, enhanced resolution, and high-mass ranges have enabled materials scientists

to characterize molecules of high mass-to-charge ratios ( $m/z$  few 100 kDa) by MS. Most often the molecules are ionized in negative-ion mode, and there are a limited number of molecules available that have the potential to act as negative-ion standards beyond  $m/z$  3000, although in some cases, calibrations have been performed by suitable salt sprays (mostly Cs-based salts) that form salt aggregates and can be ionized in both positive- and negative-ion modes.<sup>14</sup> The main problem with such a salt spray is the amount of salt required to get a series of well-defined peaks in the desired mass range (up to  $m/z$  7–8 kDa in negative-ion mode). Most often, very high concentrations of such salts (15–20 mg/mL or 15 000–20 000 ppm) are required, which are beyond the acceptable limit for any sensitive mass spectrometer.

Recently, a large number of materials have been solely characterized, and their compositions, including their inherent

Received: May 22, 2018

Accepted: August 31, 2018

Published: August 31, 2018



charges, have been determined by MS. Because of the lack of proper standards in the higher-mass range in negative-ion mode, it is often a difficult task to get the desired signal-to-noise ratio, the proper peak shape, and enough ion intensity with lower concentrations. Mass shifts in the higher-mass range can also be an issue in certain cases.

Atomically precise clusters are a new class of materials often characterized by MS.<sup>10,15–20</sup> They have molecule-like compositions and well-defined isotopic distributions, which enable their compositional identification via MS. Most of the clusters show a single peak corresponding to the molecular ion, although multiple charge states are also observed in a few cases. Many of these clusters are studied by single-crystal X-ray crystallography, and their compositions are further confirmed by MS. Several clusters of high molecular masses have also been detected in positive-ion mode with CsOAc as the ionization enhancer.<sup>15</sup> A large number of such clusters exist that show well-defined signals in negative-ion mode, such as  $\text{Au}_{25}(\text{SR})_{18}$ ,<sup>21</sup>  $\text{Ag}_{25}(\text{SR})_{18}$ ,<sup>22,23</sup>  $\text{Ag}_{29}(\text{S}_2\text{R})_{12}$ ,<sup>24,25</sup>  $\text{Ag}_{44}(\text{SR})_{30}$ ,<sup>26–28</sup> and others. Gold clusters as big as  $\text{Au}_{940\pm 20}(\text{SCH}_2\text{CH}_2\text{Ph})_{160\pm 4}$  with a molecular ion of 207 kDa, could also be detected by electrospray-ionization mass spectrometry (ESI MS), which covers  $m/z$  ranges up to 60 kDa with four charged states of the species.<sup>29</sup> All these findings suggest that these clusters can potentially be used as standards in negative-ion MS. Several clusters are known to be ionized in positive-ion mode as well, which will allow them to be used as general mass-spectrometric standards for both ESI MS as well as matrix-assisted-laser-desorption-ionization (MALDI) MS.<sup>15,30,31</sup>

Besides having well-defined mass-spectral features, a molecule should possess the following essential characteristics to be a standard: (a) The molecule of interest should be stable in the condensed state as well as in the gas phase. It should be stable in normal temperature conditions, at which typical mass spectrometers work. As discussed above, clusters are known to show stability in these conditions. (b) Purity is essential for any molecule to be a standard. As the clusters can be crystallized, purity will not be an issue. (c) Cost effectiveness is another parameter that can be achieved by using clusters as standards. For a standard-cluster synthesis, about a few tens of dollars can produce a few milligrams of such clusters. (d) The molecule should be ionizable and detectable by different mass-spectrometric techniques, such as ESI MS, MALDI MS, and others. Clusters meet this criterion also. Although there are several other criteria to satisfy for a molecule to be a standard, we have just listed a few of them. Some others are discussed in the subsequent sections.

As monolayer-protected clusters meet the essential criteria, we have taken a few such clusters and performed ESI MS qualitatively and quantitatively. In this paper, we present detailed mass-spectrometric characterization of three clusters, namely,  $[\text{Ag}_{29}(\text{BDT})_{12}]^{3-}$  (BDT: 1,3-benzene dithiol),<sup>24</sup>  $[\text{Ag}_{25}(\text{DMBT})_{18}]^{-}$  (DMBT: 2,4-dimethylbenzene thiol),<sup>22</sup> and  $[\text{Au}_{25}(\text{PET})_{18}]^{-}$  (PET: phenylethanethiol),<sup>21</sup> which can be used as standards. The required modes of calibration, such as  $m/z$  calibration, intensity calibration, voltage calibration, MS/MS calibration, and ion-mobility calibration, are presented. This study will help to overcome the unavailability of negative-ion standards for high-mass ranges. This will also introduce a new application for such clusters. With the advancement of instrumentation and commercialization of state-of-the-art equipment, the mass-spectrometric research

endeavor in materials science is inevitable, and hence the use of such clusters as standard molecules will benefit both MS as well as materials science.

## MATERIALS AND METHODS

**Materials.** Silver nitrate ( $\text{AgNO}_3$ ), dichloromethane (DCM), phenylethanethiol (PET), 2,4-dimethylbenzene thiol (DMBT), 1,3-benzene dithiol (BDT), and sodium borohydride ( $\text{NaBH}_4$ ) were purchased from Sigma-Aldrich. Chloroauric acid ( $\text{HAuCl}_4 \cdot 3\text{H}_2\text{O}$ ) was prepared in the lab from pure gold.

At present, these clusters are not commercially available. They can be synthesized easily in a chemical laboratory following the well-established modified-Brust-synthesis method.<sup>32,33</sup> Synthesis of the three clusters described in this manuscript are presented below.

**Synthesis of  $[\text{Au}_{25}(\text{PET})_{18}]^{-}$ .** This cluster was synthesized following a previously reported method with slight modification.<sup>34,35</sup> Briefly, 40 mg of  $\text{HAuCl}_4 \cdot 3\text{H}_2\text{O}$  was dissolved in 7.5 mL of THF, and 65 mg of TOABr was mixed with the solution. The resulting mixture was stirred for around 15 min until the color of the solution changed to orange red. To this solution, 68  $\mu\text{L}$  of PET was added, and it was stirred for 1 h. The as-formed Au-PET thiolate was then reduced by adding about 39 mg of  $\text{NaBH}_4$  dissolved in ice-cold water. The color of the reaction mixture changed from yellow to brown, indicating reduction of thiolates. The solution was stirred for another 5 h for complete conversion and size focusing to achieve a high yield of  $[\text{Au}_{25}(\text{PET})_{18}]^{-}$ . After 5 h, the as-synthesized cluster was dried by a rotavapor, and excess MeOH was added to it to get rid of free thiol and excess thiolates. This process was repeated a few times to get a clean cluster sample. Then, the cluster was extracted in acetone and centrifuged. The supernatant solution was collected, leaving behind a smaller quantity of precipitate consisting of larger clusters. The acetone solution was then vacuum-dried. Finally the cluster was dissolved in DCM and centrifuged at 10 000 rpm, and the supernatant solution, which consisted of the pure cluster, was collected. The purified cluster was characterized by UV-vis-absorption spectroscopy, where characteristic peaks at 675 and 450 nm confirmed the formation of  $\text{Au}_{25}$  clusters (Figure S1). The sample was crystallized from a mixture of toluene/ethanol and kept at room temperature. This sample was used for detailed characterization by ESI MS.

**Synthesis of  $[\text{Ag}_{29}(\text{BDT})_{12}(\text{TPP})_4]^{3-}$ .** This cluster was synthesized according to the reported method.<sup>24,25</sup> About 20 mg of  $\text{AgNO}_3$  was dissolved in a 15 mL mixture of 1:2 (v/v) MeOH/DCM. To this solution, 13.5  $\mu\text{L}$  of 1,3-BDT was added, which immediately resulted in a turbid yellow solution indicating the formation of insoluble Ag-S complexes. This was followed by the addition of 200 mg of PPh<sub>3</sub> in 1 mL of DCM, and the solution became colorless. The reaction mixture was stirred for about 15 min, and a freshly prepared solution of 10.5 mg of  $\text{NaBH}_4$  in 500  $\mu\text{L}$  of water was added to the mixture. The reaction mixture was kept in the dark and stirred for another 3 h while the dark-brown solution changed to orange. After 3 h, the reaction mixture was centrifuged, and the supernatant, consisting of unreacted thiolates and PPh<sub>3</sub>, was discarded. The precipitate, consisting of the  $\text{Ag}_{29}$  cluster, was washed repeatedly with methanol to remove all the impurities. The purified sample was vacuum-dried and stored in a refrigerator. Dark-orange crystals of the cluster were obtained by dropcasting a concentrated solution of the cluster in DMF

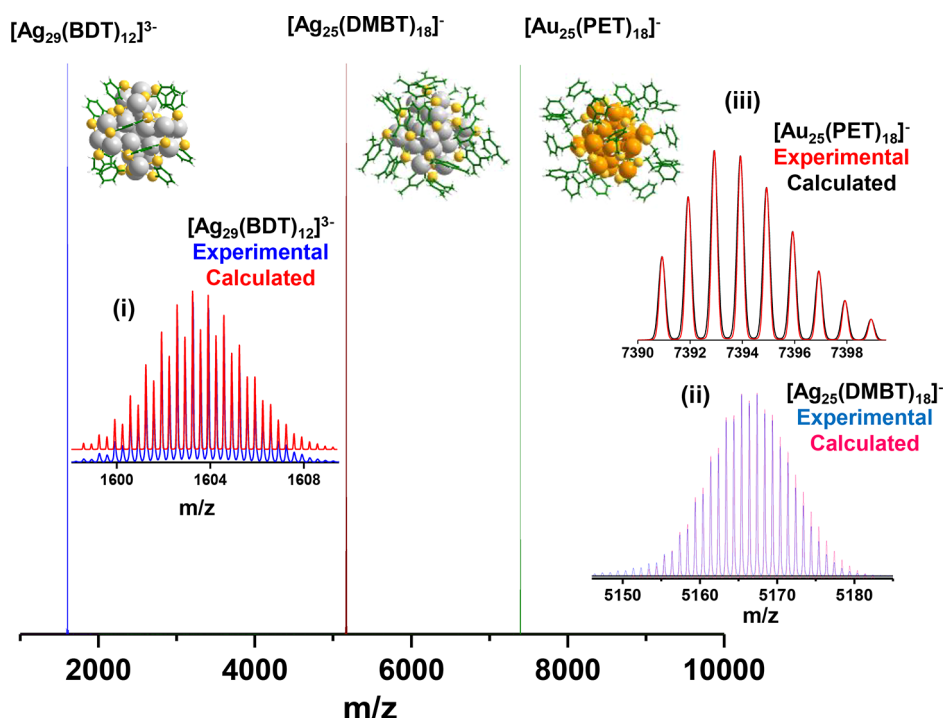


**Figure 1.** ESI MS of  $[\text{Ag}_{29}(\text{BDT})_{12}]^{3-}$ ,  $[\text{Ag}_{25}(\text{DMBT})_{18}]^{-}$ , and  $[\text{Au}_{25}(\text{PET})_{18}]^{-}$  in negative-ion mode. The clusters were analyzed separately, and their respective mass spectra are overlaid in the figure, showing that a wide range of  $m/z$  calibration is possible by using these clusters as standards. Each ion shows an exact match with its calculated isotope pattern. The structures of the clusters are represented near their molecular-ion peaks. Gray: Ag, orange: Au, yellow: S, green: C, white: H.

on a glass slide. The purified cluster was characterized by UV–vis absorption (Figure S2) and used for ESI MS studies.

**Synthesis of  $[\text{Ag}_{25}(\text{DMBT})_{18}]^{-}$ .** This synthesis followed a reported protocol with slight modification.<sup>23,34</sup> About 38 mg of  $\text{AgNO}_3$  was dissolved in a mixture of 2 mL of methanol and 17 mL of DCM, and 90  $\mu\text{L}$  of 2,4-DMBT was added to it to form yellow, insoluble Ag–S complexes; the mixture was stirred at 0 °C. After about 15–17 min, 6 mg of  $\text{PPh}_4\text{Br}$  in 0.5 mL of methanol was added. This was followed by the dropwise addition of a solution of 15 mg of  $\text{NaBH}_4$  in 0.5 mL of ice-cold water. The reaction mixture was stirred for about 7–8 h. After that, stirring was discontinued, and the solution was kept at 4 °C for about 2 days. For purification of the cluster, the sample was centrifuged to remove any insoluble impurities, and DCM was removed by rotary evaporation. The precipitate was washed twice with methanol. After that, the cluster was redissolved in DCM and again centrifuged to remove any further insoluble contaminants. DCM was again removed by rotary evaporation, and the purified cluster was obtained in the powder form. Dark-black crystals of the cluster were obtained from a DCM/hexane mixture kept at 4 °C over a period of 2–7 days. The cluster was redissolved in DCM, characterized by UV–vis (Figure S3), and then used for ESI MS.

**Instrumental Details.** All the experiments described in this work were carried out in a Waters’ Synapt G2Si HDMS instrument. The Synapt instrument consists of an electrospray source, quadrupole ion guide and trap, ion-mobility cell, and TOF detector. Different gases were used in different parts of the instrument. Nitrogen gas was used as the nebulizer gas. High-purity  $\text{N}_2$  was used in the ion-mobility cell, and the ions were directed through a drift tube. To reduce collision-induced fragmentation, He was used as the curtain gas before the ions entered the mobility cell. High-purity Ar gas was used for

collision-induced dissociation (CID). All the experiments were done in negative-ion mode. About 1  $\mu\text{g}/\text{mL}$  cluster ( $[\text{Ag}_{25}(\text{DMBT})_{18}]^{-}$  and  $[\text{Au}_{25}(\text{PET})_{18}]^{-}$ ) solution was prepared in DCM and directly infused with a flow rate of 10  $\mu\text{L}/\text{min}$ . Either DMF or ACN was used for  $[\text{Ag}_{29}(\text{BDT})_{12}]^{3-}$ . Minimum capillary voltage was applied to get a well-resolved mass spectrum. Other parameters used for analysis will be described in the course of the discussion. The instrument is highly sensitive to low concentrations of sample and can detect clusters down to 1  $\mu\text{M}$  concentrations.

Ions were analyzed by a time-of-flight mass analyzer. It has stacked ion optics to guide the ions to travel a specific path length depending on the acquisition-mode selected. Normally, ions move in a “V” path and the resolution obtained is in the range of 20 000–35 000. If required, ions can be deflected by an ion mirror to follow a “W” path where a resolution up to 50 000 can be achieved. Depending on the requirement, four different resolution modes can be selected, namely, sensitivity mode, resolution mode, high-resolution mode, and enhanced-resolution mode. In sensitivity mode, ions move in a shorter “V” path, the average resolution obtained for clusters is on the order of 15 000–20 000, low-concentration samples (1–10  $\mu\text{M}$ ) are sufficient to get the desired signal, and isotopic peaks might not be resolved to the baseline. In resolution mode, ions move in a longer “V” path, the average resolution obtained for clusters is on the order of 20 000–35 000, moderate concentrations (10–100  $\mu\text{M}$ ) are required to get good S/N, and isotopic peaks are well-resolved for all clusters with all types of charge states. In high-resolution and enhanced-resolution modes, ions move in shorter and longer “W” paths, respectively; the average resolution obtained for clusters is on the order of 35 000–50 000; and higher concentrations (1–10 mM) are required to get good S/N.

As we have obtained good resolution and S/N in resolution mode, we have performed all the experiments in this mode.

## RESULTS AND DISCUSSION

Calibration was performed using three of the above-mentioned clusters. For easier understanding, we have divided the calibration in the following parts: **Mass Calibration**, **Intensity Calibration**, **MS/MS Calibration**, and **Ion-Mobility (IM) Calibration**.

**Mass Calibration.** ESI MS of the samples was performed in the mass range of  $m/z$  100–10 000. Figure 1 shows the expanded mass spectra in the range of  $m/z$  1000–10 000. For the  $\text{Ag}_{29}(\text{BDT})_{12}(\text{TPP})_4$  cluster, a sharp peak appears at  $m/z$  1603.31, which corresponds to  $[\text{Ag}_{29}(\text{BDT})_{12}]^{3-}$ .<sup>24</sup> The TPP ligands were labile, and hence they were lost during ionization. The isotope pattern obtained matches exactly with the calculated one as shown in Figure 1 (inset i). On the other hand,  $[\text{Ag}_{25}(\text{DMBT})_{18}]^-$  shows a single peak at  $m/z$  5167.39<sup>22</sup>, and  $[\text{Au}_{25}(\text{PET})_{18}]^-$  shows a single peak at  $m/z$  7392.92. All the experimental and calculated spectra matched exactly, as shown in Figure 1 (insets ii and iii). The peak positions refer to the maximum-intensity peaks of the isotopologues.

All of these clusters can be used to calibrate the mass spectrometer. Details of the peak envelope with relative abundances and  $m/z$  positions are listed in Table S1.

**Intensity Calibration. Concentration versus Intensity.** Each of the three clusters followed almost a sigmoidal increase of the ion intensity with concentration, and the mass spectra were collected at the same instrumental conditions. Figure 2 shows the plots of normalized intensity versus concentration ( $\mu\text{M}$ ) of the clusters. The parameters were kept similar to create a simplified tune file that can be used for any general

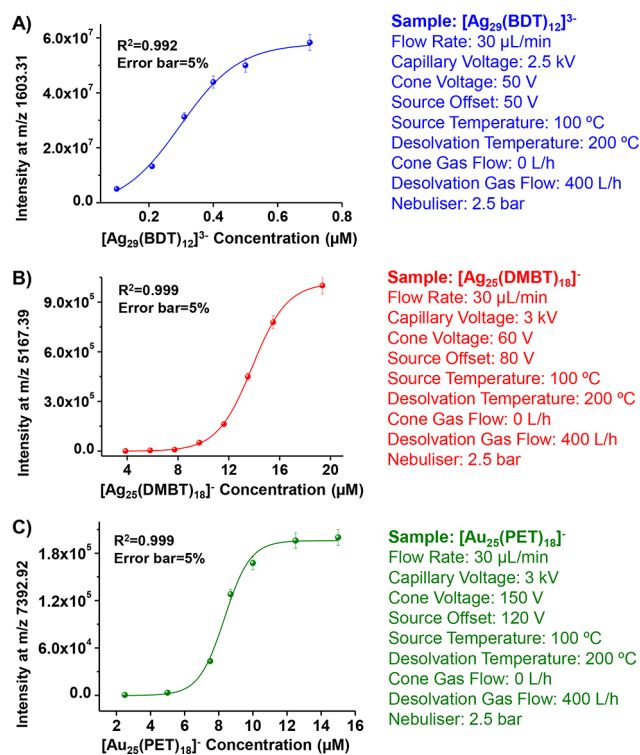


**Figure 2.** Concentration vs intensity of (A)  $[\text{Ag}_{29}(\text{BDT})_{12}]^{3-}$ , (B)  $[\text{Ag}_{25}(\text{DMBT})_{18}]^-$ , and (C)  $[\text{Au}_{25}(\text{PET})_{18}]^-$ . Optimized experimental conditions are listed along with each plot.

sample that is ionizable in negative-ion mode. Essential parameters are listed alongside the plots for the respective clusters. The same numbers of scans were averaged to avoid any error in intensity calculation.

**Voltage versus Intensity.** The maximum intensity of the desired ion was measured for the entire range of voltages. All of these clusters show increases in signal intensity with increasing capillary voltage (or ion-spray voltage) up to a certain voltage (around 3–3.5 kV). Beyond this, clusters start fragmenting because of high voltage and in-source fragmentation, resulting in decreases in ion intensity, as shown in Figure 3A–C. All the

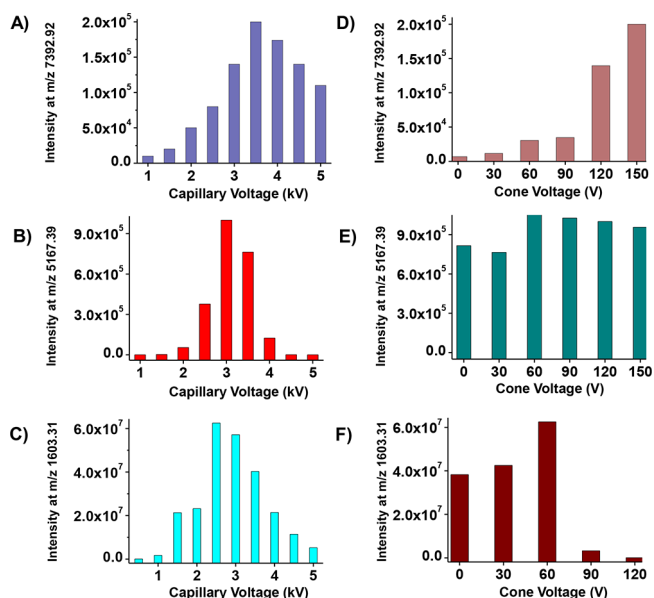


**Figure 3.** Capillary voltage vs intensity of (A)  $[\text{Au}_{25}(\text{PET})_{18}]^-$ , (B)  $[\text{Ag}_{25}(\text{DMBT})_{18}]^-$ , and (C)  $[\text{Ag}_{29}(\text{BDT})_{12}]^{3-}$ . (D–F) Dependence of cone voltage.

experiments were performed thrice and average intensity was plotted. Extraction voltage also plays a certain role in ion intensity.<sup>36,37</sup> Higher extraction voltage can also lead to fragmentation for certain molecules. However, some ions are stable throughout the extraction-voltage window. Extraction voltage also can be used to extract a preferred ion with a selective charge state. Some ions form weak dimers or polymers or gas-phase adducts, which might break if higher extraction voltages are used. For a certain molecule, choosing a certain extraction voltage is important to avoid any voltage-induced deformation as well as fragmentation.<sup>38</sup> Similarly, bias voltage may also be efficiently used for selecting a specific charge state of a selected ion. For example, for selecting a certain ion with a higher charge state, lesser bias voltage may be useful or vice versa. In the present study, capillary voltage corresponding to maximum intensity for each ion (Figure 3A–C) was selected to study the correlation with the cone (or extraction) voltage (Figure 3D–F). Although  $[\text{Au}_{25}(\text{PET})_{18}]^-$  shows a steady increase in intensity with increases in cone voltage,  $[\text{Ag}_{25}(\text{DMBT})_{18}]^-$  did not show such a dependence. On the other hand,  $[\text{Ag}_{29}(\text{BDT})_{12}]^{3-}$  showed increased intensity until 60 V, and then in-source fragmentation occurred and the intensity decreased drastically.

**MS/MS Calibration.** Each molecule has its well-defined fragmentation pattern, which is often used as a fingerprint for the molecule.<sup>39,40</sup> For unknown biomolecules, it is often

practiced that MS/MS spectra at different collision energies are collected and then matched with the reported database. For such types of molecules, exact mass is one of the most required criteria. This applies to the fragments also. Although there are several databases existing for small and large molecules and also a number of standards are available for calibration of MS/MS in positive-ion mode, very few molecules are used in negative-ion mode. The number is even smaller in the high-mass range. High concentrations of salt/salt mixtures (CsI/NaI) are mostly used for high-mass calibration.<sup>41,42</sup> These salts form (CSI)<sub>n</sub>I<sup>-</sup>-type clusters, which can cover a wide range, although this is highly dependent on the concentration used. Although *m/z* or intensity calibration is possible with these molecules, MS/MS calibration is tricky. Monolayer-protected clusters can be used to overcome this issue. Most of the clusters have well-defined fragmentation patterns that cover a low- to high-mass range. For example, [Au<sub>25</sub>(PET)<sub>18</sub>]<sup>-</sup> loses one Au<sub>4</sub>(PET)<sub>4</sub> unit, which is a neutral loss. The corresponding daughter ion, [Au<sub>21</sub>(PET)<sub>14</sub>]<sup>-</sup>, is detected at *m/z* 6056.89. Further fragmentation leads to the loss of two R groups (-SR=PET), and the fragment ion is observed at *m/z* 5846.05. These three peaks appear at higher intensities along with several other low-intensity fragments. Detailed assignment of all the peaks can be seen elsewhere<sup>43</sup> and is not in the scope of this study. Smaller thiolate fragments are seen at *m/z* 471.12 (Au(PET)<sub>2</sub><sup>-</sup>), 805.14 (Au<sub>2</sub>(PET)<sub>3</sub><sup>-</sup>), 1139.12 (Au<sub>3</sub>(PET)<sub>4</sub><sup>-</sup>), and others. Relative intensities of the peaks vary with collision energy. Fragmentation patterns at two different collision energies are shown in Figure 4A. A similar study was

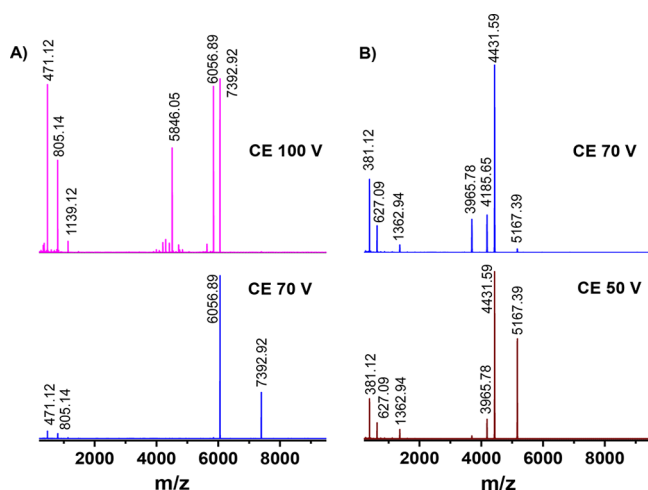


**Figure 4.** (A) CID of [Au<sub>25</sub>(PET)<sub>18</sub>]<sup>-</sup> at CE 70 and 100 V (laboratory CE), showing fragments. Exact masses of the fragments are given. (B) Similar study on [Ag<sub>25</sub>(DMBT)<sub>18</sub>]<sup>-</sup>, showing its fragments.

performed on [Ag<sub>25</sub>(DMBT)<sub>18</sub>]<sup>-</sup>, and the mass spectra are shown in Figure 4B. The MS/MS pattern of [Ag<sub>29</sub>(BDT)<sub>12</sub>]<sup>3-</sup> can also be used similarly for calibration (Figure S4). Experimental conditions and relative intensities of the ions are tabulated in Table 1. The assignment of the peaks<sup>25,43</sup> is presented in the Supporting Information (Table S2).

**Ion-Mobility (IM) Calibration.** Lack of standards for IM MS for negative ions is also an important concern.<sup>44</sup> Most of the mass spectrometers use proteins as their internal standards. Proteins have a number of gas-phase conformers and have reproducible experimental collision-cross-section (CCS) val-

**Table 1.** Intensities and *m/z* Values of Fragments of [Au<sub>25</sub>(PET)<sub>18</sub>]<sup>-</sup>, [Ag<sub>25</sub>(DMBT)<sub>18</sub>]<sup>-</sup>, and [Ag<sub>29</sub>(BDT)<sub>12</sub>]<sup>3-</sup> during CID<sup>a</sup>

CID at <i>m/z</i> 7392.93 (Au <sub>25</sub> (PET) <sub>18</sub> <sup>-</sup> )			
CE 70 V		CE 100 V	
<i>m/z</i>	relative intensity (%)	<i>m/z</i>	relative intensity (%)
805.14	3.1	471.12	96.5
1139.12	5.2	805.14	53.2
5846.05	49.6	1139.12	65.1
6056.89	100.0	5846.05	95.5
7392.92	28.3	6056.89	100.0
		7392.92	1.4
CID at <i>m/z</i> 5167.39 (Ag <sub>25</sub> (DMBT) <sub>18</sub> <sup>-</sup> )			
CE 50 V		CE 70 V	
<i>m/z</i>	relative intensity (%)	<i>m/z</i>	relative intensity (%)
381.12	23.9	381.12	1.8
627.09	9.5	627.09	100.0
1362.94	5.5	1362.94	19.7
3965.78	1.6	3965.78	17.5
4185.65	11.6	4185.65	3.9
4431.59	100.0	4431.59	14.1
567.39	60.1	567.39	38.4
CID at <i>m/z</i> 1603.31 (Ag <sub>29</sub> (BDT) <sub>12</sub> <sup>3-</sup> )			
CE 70 V		CE 100 V	
<i>m/z</i>	relative intensity (%)	<i>m/z</i>	relative intensity (%)
959.99	53.3	959.99	100.0
1603.31	100.0	1603.31	29.0
1925.39	7.5	1925.39	6.7

<sup>a</sup>Collision energy (CE) is in instrumental units, although it is mentioned as being in volts.

ues. This makes them excellent choices as standards for ion mobility.<sup>45–48</sup> Small peptides<sup>49</sup> and clusters such as C<sub>60</sub><sup>50</sup> are also known to be used as standards for low-mass calibration. Polymeric amino acids such as polyalanine<sup>44,51</sup> can be used for calibration of ion mobility but only up to *m/z* 3000. Beyond this range, no standards are available for ion-mobility calibration in negative-ion mode, especially for ESI MS. Recent reports on the use of Au<sub>n</sub><sup>±</sup> clusters for MALDI TOF used citrate-capped monodispersed Au nanoparticles as internal standards and generated in situ clusters by laser ablation which could cover a mass range until *m/z* 15 000.<sup>52</sup> However, this in situ cluster formation from such Au nanoparticles is not possible in ESI MS.

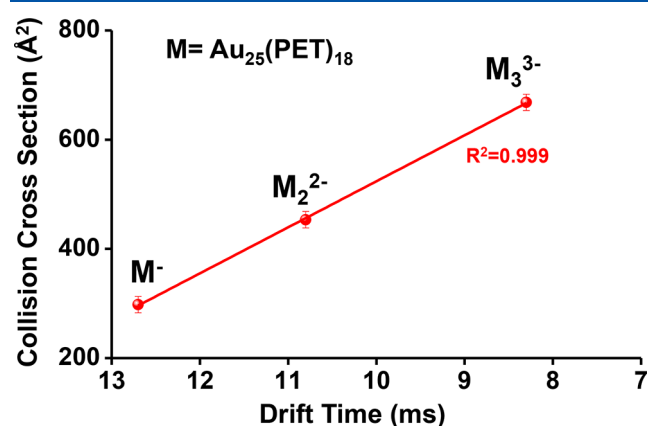
The advantages of inherent negative charge, high ionization tendency, well-defined isotope distribution, and the choice of molecules for a specific mass range make these clusters excellent standards for ion-mobility calibration. Ion-mobility drift times depend on the IMS velocity and follow a linear relation. Although the peak width changes when the IMS velocity changes, ratios of drift time (DT) and peak width (ΔDT), DT/ΔDT, should remain constant for a calibrant. We have studied the ion mobilities of all three clusters, and the data are listed in Table 2.

Drift time plots at different IMS velocities for three different clusters are shown in Figure S5. From the data, it is evident that these clusters are excellent ion-mobility standards. The [Au<sub>25</sub>(PET)<sub>18</sub>]<sup>-</sup> cluster can form polymers that are easily separable by ion mobility, and hence extended-mass-range calibration is also possible. This can be used to calibrate the

**Table 2.** Ion-Mobility-Calibration Table of  $[\text{Au}_{25}(\text{PET})_{18}]^{-}$ ,  $[\text{Ag}_{25}(\text{DMBT})_{18}]^{-}$ , and  $[\text{Ag}_{29}(\text{BDT})_{12}]^{3-}$ 

IMS calibration with $[\text{Au}_{25}(\text{PET})_{18}]^{-}$				
IMS velocity (m/s)	DT (ms)	$\Delta\text{DT}$	DT/ $\Delta\text{DT}$	intensity
400	8.99	0.535	16.80	269 000
500	12.17	0.720	16.87	144 000
600	15.90	0.950	16.73	65 000
IMS calibration with $[\text{Ag}_{25}(\text{DMBT})_{18}]^{-}$				
IMS velocity (m/s)	DT (ms)	$\Delta\text{DT}$	DT/ $\Delta\text{DT}$	intensity
400	8.02	0.829	9.67	237 000
500	10.51	1.082	9.71	195 000
600	13.41	1.385	9.68	130 000
IMS calibration with $[\text{Ag}_{29}(\text{BDT})_{12}]^{3-}$				
IMS velocity (m/s)	DT (ms)	$\Delta\text{DT}$	DT/ $\Delta\text{DT}$	intensity
400	2.01	0.244	8.23	269,000,00
500	2.56	0.273	9.37	245,000,00
600	3.05	0.336	9.07	219,000,00

CCS for the system. Dimers and trimers of  $[\text{Au}_{25}(\text{PET})_{18}]^{-}$  form at specific instrumental conditions, and all these polymers appear at the same  $m/z$ .<sup>34</sup> Drift time versus CCS follows a linear correlation for these species. As they are at the same  $m/z$  with different charges, it is easy to calibrate the CCS using these polymers (see Figure 5).

**Figure 5.** Drift time vs collision cross section (CCS) of  $\text{Au}_{25}(\text{PET})_{18}^{-}$  monomer, dimer, and trimer showing a linear relationship.

## CONCLUSION

In this paper, we tried to emphasize the use of monolayer-protected clusters as MS standards, taking three well-established clusters as examples. These clusters are shown to be used as calibrants for  $m/z$ , intensity, MS/MS, IMS, and CCS measurements. These cover most of the aspects of samples measured in ESI MS. Although only three clusters are shown as potential standards for negative-ion MS, this should not be seen as a limitation. Several clusters are reported and many of them are known to form crystals. At present, clusters with 900 metal atoms and masses exceeding 100 kDa are available, and they are detectable by MS as well. These clusters can also be used for calibrating higher-mass ranges. Another advantage of using these materials as standards is the use of them for MALDI MS; this aspect has not been studied in the present manuscript. These clusters are stable in the laser-desorption process. There has been a tremendous increase in

the number of publications in which MS is used to characterize materials. As cluster science is expanding and new molecules are being added each day, standardization of mass spectrometers for the study of clusters is indeed a necessity for the future of materials science.

## ASSOCIATED CONTENT

### Supporting Information

The Supporting Information is available free of charge on the ACS Publications website at DOI: 10.1021/acs.analchem.8b02280.

UV-vis characterization of the clusters, additional ESI MS, details of the peak envelope of the isotope pattern, and assignment of the fragments obtained in the MS/MS spectra of the clusters (PDF)

## AUTHOR INFORMATION

### Corresponding Author

\*E-mail: pradeep@iitm.ac.in. Fax: 91-44-2257-0545/0509.

### ORCID

Thalappil Pradeep: 0000-0003-3174-534X

### Present Address

†A.B.: Karlsruhe Institute of Technology (KIT), Institute of Nanotechnology, Hermann-von-Helmholtz-Platz 1, 76344 Eggenstein-Leopoldshafen, Germany.

### Author Contributions

‡A.B. and P.C. contributed equally. The manuscript was written through the contributions of all authors.

### Notes

The authors declare no competing financial interest.

## ACKNOWLEDGMENTS

A.B. thanks Indian Institute of Technology Madras (IITM) for an institute postdoctoral fellowship. P.C. thanks the Council of Scientific and Industrial Research (CSIR) for a research fellowship. A.N., D.G., and S.B. thank IITM for institute doctoral fellowships.

## REFERENCES

- (1) Mann, M. *Nat. Rev. Mol. Cell Biol.* **2016**, *17*, 678.
- (2) Rauschenbach, S.; Ternes, M.; Harnau, L.; Kern, K. *Annu. Rev. Anal. Chem.* **2016**, *9*, 473–498.
- (3) Sauer, S.; Kliem, M. *Nat. Rev. Microbiol.* **2010**, *8*, 74–82.
- (4) Zheng, Q.; Chen, H. *Annu. Rev. Anal. Chem.* **2016**, *9*, 411–448.
- (5) Eberlin, L. S.; Tibshirani, R. J.; Zhang, J.; Longacre, T. A.; Berry, G. J.; Bingham, D. B.; Norton, J. A.; Zare, R. N.; Poultides, G. A. *Proc. Natl. Acad. Sci. U. S. A.* **2014**, *111*, 2436–2441.
- (6) Eberlin, L. S.; Norton, I.; Orringer, D.; Dunn, I. F.; Liu, X.; Ide, J. L.; Jarmusch, A. K.; Ligon, K. L.; Jolesz, F. A.; Golby, A. J.; Santagata, S.; Agar, N. Y. R.; Cooks, R. G. *Proc. Natl. Acad. Sci. U. S. A.* **2013**, *110*, 1611–1616.
- (7) Ifá, D. R.; Eberlin, L. S. *Clin. Chem.* **2016**, *62*, 111–123.
- (8) Sztaray, J.; Memboeuf, A.; Drahos, L.; Vekey, K. *Mass Spectrom. Rev.* **2011**, *30*, 298–320.
- (9) Chace, D. H. *Chem. Rev.* **2001**, *101*, 445–477.
- (10) Chakraborty, I.; Pradeep, T. *Chem. Rev.* **2017**, *117*, 8208–8271.
- (11) Krishnadas, K. R.; Baksi, A.; Ghosh, A.; Natarajan, G.; Som, A.; Pradeep, T. *Acc. Chem. Res.* **2017**, *50*, 1988–1996.
- (12) Pradeep, T.; Baksi, A.; Xavier, P. L. *RSC Smart Mater.* **2014**, *7*, 169–225.
- (13) Xavier, P. L.; Chaudhari, K.; Baksi, A.; Pradeep, T. *Nano Rev.* **2012**, *3*, 14767.

- (14) Galhena, A. S.; Jones, C. M.; Wysocki, V. H. *Int. J. Mass Spectrom.* **2009**, *287*, 105–113.
- (15) Jin, R.; Zeng, C.; Zhou, M.; Chen, Y. *Chem. Rev.* **2016**, *116*, 10346–10413.
- (16) Maity, P.; Xie, S.; Yamauchi, M.; Tsukuda, T. *Nanoscale* **2012**, *4*, 4027–4037.
- (17) Kurashige, W.; Niihori, Y.; Sharma, S.; Negishi, Y. *Coord. Chem. Rev.* **2016**, *320–321*, 238–250.
- (18) Gerwien, A.; Schildhauer, M.; Thumser, S.; Mayer, P.; Dube, H. *Nat. Commun.* **2018**, *9*, 1–9.
- (19) Yao, Q.; Feng, Y.; Fung, V.; Yu, Y.; Jiang, D.-e.; Yang, J.; Xie, J. *Nat. Commun.* **2017**, *8*, 1–11.
- (20) Yao, Q.; Yuan, X.; Fung, V.; Yu, Y.; Leong, D. T.; Jiang, D.-e.; Xie, J. *Nat. Commun.* **2017**, *8*, 1–11.
- (21) Zhu, M.; Aikens, C. M.; Hollander, F. J.; Schatz, G. C.; Jin, R. *J. Am. Chem. Soc.* **2008**, *130*, 5883–5885.
- (22) Joshi, C. P.; Bootharaju, M. S.; Alhilaly, M. J.; Bakr, O. M. *J. Am. Chem. Soc.* **2015**, *137*, 11578–11581.
- (23) Krishnadas, K. R.; Baksi, A.; Ghosh, A.; Natarajan, G.; Pradeep, T. *Nat. Commun.* **2016**, *7*, 13447.
- (24) AbdulHalim, L. G.; Bootharaju, M. S.; Tang, Q.; Del Gobbo, S.; AbdulHalim, R. G.; Eddaoudi, M.; Jiang, D.-e.; Bakr, O. M. *J. Am. Chem. Soc.* **2015**, *137*, 11970–11975.
- (25) Chakraborty, P.; Baksi, A.; Khatun, E.; Nag, A.; Ghosh, A.; Pradeep, T. *J. Phys. Chem. C* **2017**, *121*, 10971–10981.
- (26) Desireddy, A.; Conn, B. E.; Guo, J.; Yoon, B.; Barnett, R. N.; Monahan, B. M.; Kirschbaum, K.; Griffith, W. P.; Whetten, R. L.; Landman, U.; Bigioni, T. P. *Nature* **2013**, *501*, 399–402.
- (27) Yang, H.; Wang, Y.; Huang, H.; Gell, L.; Lehtovaara, L.; Malola, S.; Hakkinen, H.; Zheng, N. *Nat. Commun.* **2013**, *4*, 2422.
- (28) Baksi, A.; Ghosh, A.; Mudedla, S. K.; Chakraborty, P.; Bhat, S.; Mondal, B.; Krishnadas, K. R.; Subramanian, V.; Pradeep, T. *J. Phys. Chem. C* **2017**, *121*, 13421–13427.
- (29) Kumara, C.; Zuo, X.; Cullen, D. A.; Dass, A. *ACS Nano* **2014**, *8*, 6431–6439.
- (30) Sakthivel, N. A.; Theivendran, S.; Ganeshraj, V.; Oliver, A. G.; Dass, A. *J. Am. Chem. Soc.* **2017**, *139*, 15450–15459.
- (31) Kumara, C.; Zuo, X.; Ilavsky, J.; Chapman, K. W.; Cullen, D. A.; Dass, A. *J. Am. Chem. Soc.* **2014**, *136*, 7410–7417.
- (32) Brust, M.; Walker, M.; Bethell, D.; Schiffrin, D. J.; Whyman, R. *J. Chem. Soc., Chem. Commun.* **1994**, *0*, 801–802.
- (33) Chakraborty, I.; Pradeep, T. *Chem. Rev.* **2017**, *117*, 8208–8271.
- (34) Baksi, A.; Chakraborty, P.; Bhat, S.; Natarajan, G.; Pradeep, T. *Chem. Commun.* **2016**, *52*, 8397–8400.
- (35) Bhat, S.; Baksi, A.; Mudedla, S. K.; Natarajan, G.; Subramanian, V.; Pradeep, T. *J. Phys. Chem. Lett.* **2017**, *8*, 2787–2793.
- (36) Pashynska, V. A.; Kosevich, M. V.; Heuvel, H. V. d.; Claeys, M. *Rapid Commun. Mass Spectrom.* **2006**, *20*, 755–763.
- (37) Hunt, S. M.; Sheil, M. M.; Belov, M.; Derrick, P. *Anal. Chem.* **1998**, *70*, 1812–1822.
- (38) Yan, Z.; Caldwell, G. W.; Jones, W. J.; Masucci, J. A. *Rapid Commun. Mass Spectrom.* **2003**, *17*, 1433–1442.
- (39) Dührkop, K.; Shen, H.; Meusel, M.; Rousu, J.; Böcker, S. *Proc. Natl. Acad. Sci. U. S. A.* **2015**, *112*, 12580.
- (40) Cottrell, J. S. *J. Proteomics* **2011**, *74*, 1842–1851.
- (41) Lou, X.; van Dongen, J. L. J.; Meijer, E. W. *J. Am. Soc. Mass Spectrom.* **2010**, *21*, 1223–1226.
- (42) König, S.; Fales, H. M. *J. Am. Soc. Mass Spectrom.* **1999**, *10*, 273–276.
- (43) Angel, L. A.; Majors, L. T.; Dharmaratne, A. C.; Dass, A. *ACS Nano* **2010**, *4*, 4691–4700.
- (44) Forsythe, J. G.; Petrov, A. S.; Walker, C. A.; Allen, S. J.; Pellissier, J. S.; Bush, M. F.; Hud, N. V.; Fernandez, F. M. *Analyst* **2015**, *140*, 6853–6861.
- (45) Kune, C.; Far, J.; De Pauw, E. *Anal. Chem.* **2016**, *88*, 11639–11646.
- (46) Chawner, R.; McCullough, B.; Giles, K.; Barran, P. E.; Gaskell, S. J.; Evers, C. E. *J. Proteome Res.* **2012**, *11*, 5564–5572.
- (47) Jurneczko, E.; Kalapothakis, J.; Campuzano, I. D. G.; Morris, M.; Barran, P. E. *Anal. Chem.* **2012**, *84*, 8524–8531.
- (48) Haler, J. R. N.; Kune, C.; Massonnet, P.; Comby-Zerbino, C.; Jordens, J.; Honing, M.; Mengerink, Y.; Far, J.; De Pauw, E. *Anal. Chem.* **2017**, *89*, 12076–12086.
- (49) Bush, M. F.; Campuzano, I. D. G.; Robinson, C. V. *Anal. Chem.* **2012**, *84*, 7124–7130.
- (50) Mesleh, M. F.; Hunter, J. M.; Shvartsburg, A. A.; Schatz, G. C.; Jarrold, M. F. *J. Phys. Chem.* **1996**, *100*, 16082–16086.
- (51) Lietz, C. B.; Yu, Q.; Li, L. *J. Am. Soc. Mass Spectrom.* **2014**, *25*, 2009–2019.
- (52) Kolářová, L.; Prokeš, L.; Kučera, L.; Hampl, A.; Peňa-Méndez, E.; Vaňhara, P.; Havel, J. *J. Am. Soc. Mass Spectrom.* **2017**, *28*, 419–427.